Study of Extensions to the Linear Sampling Method for Electromagnetic Inverse Scattering

Yeasmin Sultana
Marquette University

STUDY OF EXTENSIONS TO THE LINEAR SAMPLING METHOD FOR ELECTROMAGNETIC INVERSE SCATTERING

by

YEASMIN SULTANA

A Thesis submitted to the Faculty of the Graduate School,
Marquette University,
in Partial Fulfillment of the Requirements for
the Degree of Masters of Science (Electrical and Computer Engineering).

Milwaukee, Wisconsin

December 2021

ABSTRACT

STUDY OF EXTENSIONS TO THE LINEAR SAMPLING METHOD FOR ELECTROMAGNATIC INVERSE SCATTERING

YEASMIN SULTANA

MARQUETTE UNIVERSITY, 2021

The linear sampling method (LSM) is a simple and effective qualitative method to reconstruct the support of unknown object by solving inverse scattering problem. The solution is done based on the field radiated by the elementary source located in a set of test points. In this thesis, the LSM formulation, limitations of standard LSM and extensions of LSM are discussed. Standard LSM can reconstruct simply connected objects, but it fails in case of concave or not simply connected objects. However, it can reconstruct the convex hull for such objects. Some extensions to LSM have been proposed to avoid these limitations. Two of these extensions are generalized LSM (GLSM) and multipole based LSM (MLSM). GLSM is formulated by generalizing the right side of the linear equation to higher order multipoles. This provides more information about the radiated field. The reconstruction is even better by using some post-processing scheme such as a modified indicator function and higher values for the regularization parameter. But GLSM cannot reconstruct the actual shape for some complex objects. MLSM is based on physical regularization. This method analyzes the multipole expansion of the scattered field. Only monopole and dipole terms are used for the reconstruction. This modification shows better reconstruction than the mathematical regularization in GLSM. Another advantage of MLSM is that the threshold for boundary contour is constant for all types of objects. From the results, it is evident that MLSM is somewhat better than GLSM when the object's complex hull is very different than the object itself. However, higher permittivity affects the solutions. It can be avoided by using higher value of regularization parameter in GLSM but in MLSM there is no known remedy.

TABLE OF CONTENTS

LIST OF TABLES

LIST OF FIGURES

1. INTRODUCTION

1.1 Microwave Imaging

Microwave imaging represents a series of techniques in remote sensing and non-invasive investigation to retrieve information about the physical properties and/or condition of the structures under test. The electromagnetic field that results from the interaction between the interrogating waves and the materials is collected for testing. So, the techniques are usually based on short range measurement.

The use of electromagnetic fields for remote sensing or inspecting unknown objects has been proposed for many years as the change in relative permittivity has strong effect on scattered field. Microwave imaging is a non-ionizing and potentially low-cost imaging modality. But there are some limitations in resolution because the wavelength is on the order of size of important features.

An active imaging system consists of several elements such as an electromagnetic source, a collecting system, a processing unit, etc. A general conceptual diagram is shown in Figure 1.1. The source generates the electromagnetic waves that interact with the object when it passes through the object. Then the modified radiated waves are collected by the collecting system. These waves carry the information about the object which is carried to the processing unit. This unit investigates the waves to deduce information about the object, often in the form of an image [1].

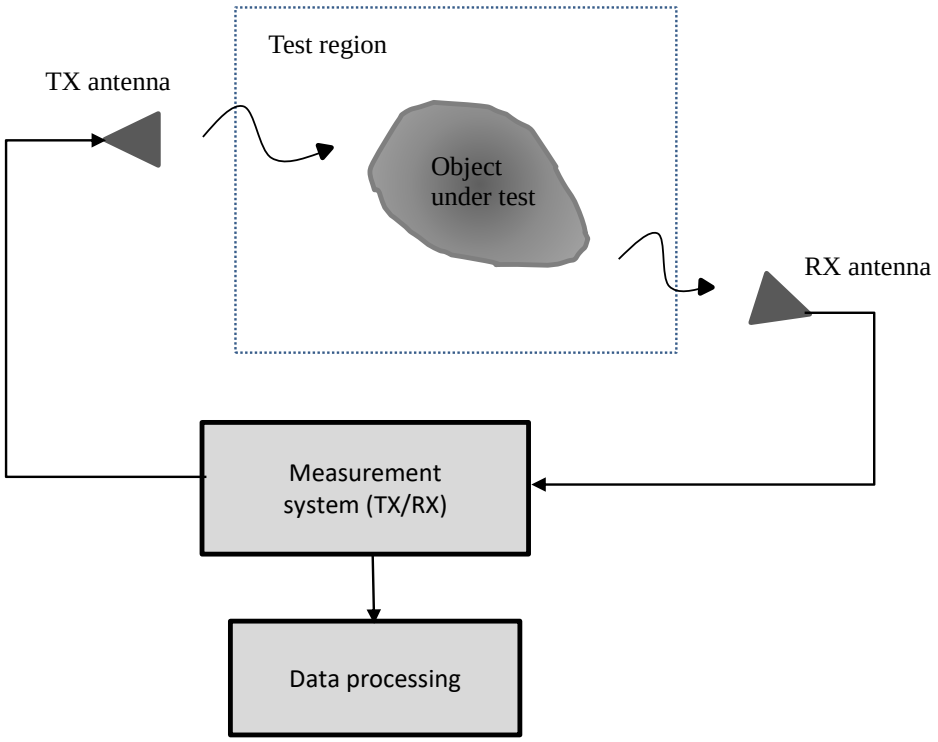

Figure 1-1 Schematic representation of a microwave imaging system

1.1.1 Microwave Frequencies

Microwaves include the frequencies ranging from 300 MHz to 300 GHz. Therefore, denoting the speed of electromagnetic waves in vacuum as v_0 and the frequency as f, the wavelength λ_0 in vacuum is defined by,

$$\lambda_0 = \frac{v_0}{f} \tag{1}$$

The microwave wavelength range is between 1 mm and 1m. These wavelengths are usually comparable to the size of the object in practical applications. Microwave frequency bands are often designated by letters that specify the frequency range of operation. Table 1.1 shows the band designation indicated by IEEE standard [2], and their relations with the frequency band designations of the International Telecommunications Union (ITU) [3].

Table 1.1 Microwave Frequency Bands

IEEE Radar Nomenclature			**ITU Nomenclature**		
Band Designation	**Frequency Range**	**Wavelength Range (Vacuum)**	**Frequency Range**	**Wavelength Range (Vacuum)**	**Band Designation**
Ultrahigh Frequency (UHF)	300-1000 MHz	30 cm-1m	300-3000 MHz	0.1-1m	Ultrahigh Frequency (UHF)
L	1-2 GHz	15-30 cm			
S	2-4 GHz	7.5-15 cm	3-30 GHz	1-10 cm	Superhigh Frequency (SHF)
C	4-8 GHz	3.75-7.5 cm			
X	8-12 GHz	2.5-3.75 cm			
Ku	12-18 GHz	1.67-2.5 cm			
K	18-27 GHz	1.11-1.67 cm			
Ka	27-40 GHz	0.75-1.11 cm	30-300 GHz	0.1-1 cm	Extremely High Frequency (EHF)
V	40-75 GHz	4-7.5 mm			
W	75-110 GHz	2.73-4 mm			
mm	110-300 GHz	1-2.72 mm			

1.1.2 Illuminating Systems

The illuminating system includes a source which operates at microwave frequencies and is usually an antenna. The incident field radiated by the source plays a key role in the reconstruction system. Sometimes there is only one illuminating source. When there are multiple sources, the object is illuminated from different positions and the

imaging is denoted as a multi-illumination configuration. For complex systems, an array of antennas is used which significantly complicates the source. Sometimes multiple frequencies are used to investigate a single object. This is called multifrequency imaging. Another approach is work in the time domain. Here the incident field has time nature and consists of multiple frequencies [1]. The incident pulse is defined by its frequency band.

1.1.3 Receiving Systems

A scattered field is generated when the incident field interacts with the object. This scattered field consists of electric and magnetic field vectors denoted by $\vec{E}^s(\vec{r})$ and $\vec{H}^s(\vec{r})$. As per definition of electromagnetic scattering, the sum of the incident and scattered fields yields the total fields.

$$\vec{E}^T(\vec{r}) = \vec{E}^i(\vec{r}) + \vec{E}^s(\vec{r})$$
$$\vec{H}^T(\vec{r}) = \vec{H}^i(\vec{r}) + \vec{H}^s(\vec{r}) \quad (2)$$

The total field is measured at the receiver when the object is present. But the scattered field contains information about the object. As the total field includes the incident and scattered field, it will only have the incident field when the object is not present. Therefore, $\vec{E}^s(\vec{r}) = 0$ and $\vec{H}^s(\vec{r}) = 0$. Thus, the scattered field is measured by subtracting the incident field from the total field. Similarly to the illuminating system, the receiving system can have single or multiple antennas. In a single frequency configuration, the receiving antenna locations coincide with the illuminating one. When a single receiving antenna receives the signal by moving around the object, it is called a bistatic configuration.

Another configuration is multistatic configuration where a set of different antennas is used for transmitting and collecting the field. The multiview configuration is used in tomographic applications where the transmitting and receiving systems are rotated mutually around the object.

1.1.4 Interaction Between the Incident Field and the Object

The interaction between the incident field and the object is governed by the electromagnetic scattering laws. This includes reflection, transmission, absorption, diffraction, and others. The interaction depends on the incident wave as well as the physical and geometrical properties of the object. Therefore, the relationship regulating the behaviors of the various materials is important in electromagnetic interactions.

In some cases, the external shape of the object is known so the imaging process is only used to retrieve information such as the distribution of dielectric permittivity, electric conductivity, and magnetic permeability. In other applications it is limited to the position of the object, possible defects or discontinuity in the structure, and so on.

When the external shape is not known, it is assumed that the object is contained in a fixed region. That region is considered as the investigation domain where the object is unknown. The interaction between the field and object also depends on the propagation medium. So, the incident field must be known inside of the investigation domain. Imaging can be done by solving a specific inverse source problem [1].

1.2 Applications

Microwave imaging techniques present unique features that allow applications to perform nondestructive evaluations and imaging. The inspection of internal incorporation of objects when it is coated or layered by dielectric materials can be done as microwaves have the capability of penetrating dielectric objects. Also, it can directly retrieve the dielectric properties of the object. This can be correlated with other physical properties or state of an object. In the last decade, engineers, scientists and professionals from both the research community and industry have focused on developing innovative solutions in the multidisciplinary area of imaging. The applications of microwave imaging in different fields are discussed briefly in this section.

1.2.1 Civil Engineering and Industrial Applications

Microwave imaging is widely used in civil and industrial applications such as material characterization, nondestructive testing, and industrial process monitoring. This is possible due to their ability to penetrate dielectric materials. The dielectric properties for materials that are used in civil and industrial fields can be determined using microwaves such as:

- Dielectric properties of concrete: the complex permittivity of the concrete is frequency dependent. It also depends on other factors as porosity, temperature and saturation of pores. Different dielectric models have been adopted [1] to represent the dielectric properties of concrete.

- Dielectric properties of plastic materials: Widespread production of plastic and controlled dielectric properties make plastics a suitable target for microwave imaging.

- Dielectric properties of food and vegetables: there has been a remarkable interest in characterization of dielectric properties of food, fruits and vegetables [4], [5], [6]. These properties can be used in moisture content estimation and quality control [7], [8].

- Dielectric properties of wood: the dielectric properties of wood help to detect defective parts such as void or rotten parts in wood trunks. In the void parts the permittivity decreases significantly. But for the rotten case the permittivity increases.

Some of the applications in civil and industrial fields [1] are:

- Imaging of civil structures: microwave imaging can be used in case of inspection of civil structures to evaluate the condition of the buildings, roads and bridges.

- Imaging of plastic materials: similar to dielectric property estimation, both quantitative and qualitative methods can be used in the imaging process.

- Imaging of wood materials: imaging of wood materials is used to detect the inclusions of metals and stones into trees which can damage cutting machinery. It can also be used to evaluate the healthy state of living trees.

- Imaging of metallic structures: imaging can be used in the inspection of composite or coated metallic parts or the detection of surface cracks in metallic structures.

- Microwave imaging can also be used in industrial applications connected to chemical, pharmaceutical, agricultural, and food production areas.

1.2.2 Biomedical Applications

Microwave imaging has significant use in diagnostic applications in the biomedical field. The preliminary proposals are mentioned in [9]. Here the characterization of biological tissues in terms of dispersion and attenuation is done based on radar and inverse scattering concepts. It can also be used to detect breast cancer and brain stroke. Dielectric properties of breast tissues: the detection of dielectric properties of normal and malignant breast tissues helps to detect tumor tissues in case of breast cancer such as:

- Dielectric properties of brain tissues: microwave imaging has significant use in case of detection and monitoring brain strokes. Therefore, there has been an increasing interest in characterizing the dielectric properties of brain tissues.

- Breast models: apart from the dielectric properties of the tissues, it is also important to create specific numerical models to create the breast models. Microwave imaging is used in this case. Specific numerical models are available from the University of Wisconsin-Madison [10], [11].

- Head models: Some of the numerical phantoms are obtained from MRI or CT images which have been properly segmented to obtain the resolutions suitable for electromagnetic simulations in microwave range.

Some of the main uses are:

- Breast imaging: one of the foremost applications of microwave imaging in biomedical field is breast imaging for cancer detection [12], [13]. Different imaging techniques are used in these cases such as beamforming-based imaging techniques and inverse scattering techniques.

- Brain stroke imaging: the detection and imaging of brain strokes at microwave frequencies have been pursued by different strategies including qualitative approach, quantitative approach base on inverse scattering [1].

- Other medical applications: microwaves have been considered for imaging purposes in other medical applications such as imaging of human forearms and monitoring medical treatment like microwave ablation. Recently it has been proposed as potential candidate to diagnosis cervical myelopathy [14].

1.2.3 Security Applications

The ability of electromagnetic waves to penetrate dielectric materials opens a wide range of possibilities for using microwave imaging in the field of security. The main applications are related to detection of concealed targets, inspection, and monitoring of inaccessible domains.

One of the main security related application is through-the-wall imaging (TWI). It attempts to identify or track targets inside buildings [15]. In this approach wall characterization is a very important part. There is usually a great variability in both adopted materials and the internal structures of a wall. Proper characterization of the wall helps to avoid masking the reflections from the wall and from hidden targets. Different approaches like beamforming techniques and inverse scattering techniques are used for TWI.

1.2.4 Subsurface Prospection Applications

Microwave imaging is used for shallow subsurface detection, including the retrieval of tunnels, pipes, and other buried objects. In this case ground penetrating radar (GPR) is widely used to receive the scattered field data. The pulsed incident field from GPR is used to illuminate the region under inspection and then the scattered field that radiated from the buried target is collected at a proper set of points. The knowledge of dielectric properties of soil is of great importance in such applications. Both linear and nonlinear inversion approaches are used in these applications [1].

These applications require any inversion approach to be computationally effective, provide fast and reliable reconstruction without detailed a priori information. But most classical approaches do not fulfill these conditions.

1.3 Microwave Scattering

Scattering of waves describes how waves interact with various objects. When an electromagnetic wave falls upon an object, it absorbs energy from the wave and reradiates

it. The re-radiated energy is centered at the scatterer. This process is called electromagnetic scattering [16].

There are two types of scattering problems that exist, the direct scattering problem and the inverse scattering problem. The direct electromagnetic scattering problem determines the scattered field where the physical and geometrical properties of the scatterer are known. The inverse problem infers information on the inhomogeneity from knowledge of the scattered wave at a large distance from the scatterer [16].

Field−matter interactions can affect the state of the scattering object and yield an electromagnetic signal that can be measured and analyzed with the purpose of retrieving useful information about the object. Rigorous solutions of the direct electromagnetic scattering problem are available for specific shapes. A numerical technique is developed in [17] for arbitrary cross section of two dimensional objects. This is based on the integral equation for the field of a harmonic source in the presence of a dielectric cylinder of arbitrary cross section shape. This approach is applicable primarily for the cross-section area of the dielectric cylinder which is not too large.

By solving the electromagnetic scattering inverse problem, the reconstruction of the structural and electromagnetic parameters of unknown targets is possible from the knowledge of the field they scatter when probed with known incident fields. It is generally an ill-posed problem. Due to the ill-posedness and nonlinearity of the data to unknown relationship, the solution is a non-trivial task. Any numerical implementation for the solution should incorporate a regularization procedure to eliminate artificial oscillations [18].

Traditional approaches to the electromagnetic scattering inverse problem can be divided into two families [16]:

- Quantitative Methods
- Qualitative Methods

1.4 Quantitative Methods

Quantitative methods are typically non-linear optimization schemes, where an iterative process is used on an initial guess of the position and shape of the scatterer [19]. These methods determine both the shape and electromagnetic contrast of the target [18]. The problem with this approach is it requires an accurate initial guess and a long reconstruction time. In many applications accurate a priori information is not available.

Other techniques use the weak scattering approximation. These methods include the Born and Kirchhoff inversion approach, where a linear inverse problem is formulated using a low or high frequency assumption [18]. This assumption helps to linearize the data-to-unknown relationship. In these approaches, the weak scattering condition is a priori information of the far scattered field. They typically provide only a rough description of the target's shape.

Methods that solve the general problem include the distorted Born iterative method [20] and the subspace optimization method [21]. These methods solve the forward problem repeatedly to solve the inverse problem. But solving the forward problem repeatedly needs a long time. Other methods such as the modified gradient method [22], [23], the contrast

source method [24], [25] can be used. Here a matrix optimization is used to solve the problem.

Some hybrid methods [26], [27], [28] are proposed to achieve the target's boundary via qualitative inversion. The result is used as a priori information for quantitative inversion. These approaches help to improve the reliability and reduce the computational burden.

1.5 Qualitative Methods

Qualitative methods provide only partial information about the object which is usually the boundary of the object. The most popular qualitative method is the linear sampling method [29]. In the linear sampling method, the non linear difficulties are avoided as the linearity does not come from an approximation based on any physical condition. Here, the linearity comes from the equivalence between the non-linear inverse scattering problem and the linear combination of experiments. For each point, a linear combination of incident and scattered fields is computed. The solution of this equation has the property that it becomes unbounded for a test point on and in the exterior of the boundary. This helps to reconstruct the shape of the inhomogeneity [30].

The main advantages of the LSM are:

- High computational speed, the use of clever sampling scheme helps to reduce the time for the reconstruction. In case of 2D reconstruction only few minutes are required. But it can take a few of hours for 3D[1].

- Very little a priori information on the scatterer is needed.

- The implementation is computationally simple as it requires only the solution of a finite number of ill-conditioned linear systems.

1.6 Motivation

The inverse scattering problem for electromagnetic waves is an area of major importance in applied mathematics as well as testing and diagnostics applications such as the reconstruction of the shape of an object where the object cannot be directly probed. Mathematically, this is an ill-posed and non-linear problem. One of the effective ways to solve this problem is the qualitative inversion methods [16], [19], [31]. In these methods the reconstruction is done by the solution of an auxiliary linear inverse problem. It is simple and computationally effective. The most popular qualitative method is the linear sampling method (LSM). It can be simply implemented as it only requires sampling the domain under test on an arbitrary grid of sampling points. Then the linear integral equation is solved for each of them. But there are some limitations of applying the LSM in practice. Due to these limitations some extensions have been proposed. In this thesis, two main extensions are investigated, and the results have been compared to find out which method gives the comparatively better reconstruction.

2. THEORY

2.1 Introduction

This chapter discusses the theory related to solving the inverse scattering problem. The inverse scattering problem formulation will be introduced in the next section. Then the use of LSM in inverse scattering is described. The limitations of LSM are reviewed. Modifications to LSM that overcome these limitations are developed at the end of the chapter.

2.2 Inverse Scattering Problem Formulation

A typical scenario is shown in Figure 2.1. There is a scatterer within a domain D. The domain D is bounded by a set of antennas. Each antenna can act as a transmitter (with incident direction labeled as inc), or as a receiver (with scattered direction labeled as scat). For each incident angle, the scattered fields at all antennas are measured. This collection of measurements is the data that is used to solve the inverse scattering problem.

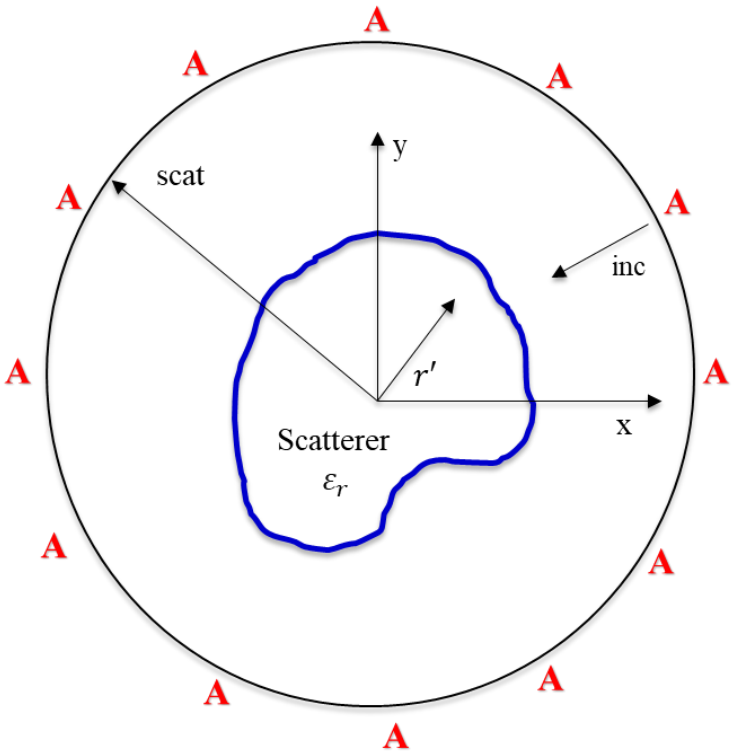

Figure 2-1 Generic geometry of the inverse scattering problem.

Here the scattered field is constructed by taking the incident field away from the total field. All these fields satisfy the Maxwell's equations. So, considering the incident field $\vec{E}^{\mathrm{i}}$ and total field $\vec{E}^{\mathrm{T}}$ for dielectric case yields [32]

$$\begin{aligned} \nabla \times \vec{E}^{i} &= -j\omega\mu_0\vec{H}^{i} & \nabla \times \vec{H}^{i} &= j\omega\varepsilon_0\vec{E}^{i} \\ \nabla \times \vec{E}^{T} &= -j\omega\mu_0\vec{H}^{T} & \nabla \times \vec{H}^{T} &= j\omega\varepsilon\vec{E}^{T} \end{aligned} \tag{3}$$

Also, the scattered field $\vec{E}^{\mathrm{s}}$ satisfies

$$\nabla \times \vec{E}^{s} = -j\omega\mu_0\vec{H}^{s} \qquad \nabla \times \vec{H}^{s} = J_{eq} + j\omega\varepsilon_0\vec{E}^{s} \tag{4}$$

where [17]

$$J_{eq} = j\omega(\varepsilon - \varepsilon_0)\vec{E}^T \tag{5}$$

Consider a 2-D problem, TM^z, where $\vec{E} = E(x, y)\hat{e}_z$. Now taking the curl of both sides of equation (4) and rearranging,

$$\nabla^2 E^s + k_b^2 E^s = -k_b^2 \chi(\vec{r})\vec{E}^T \tag{6}$$

where $\chi(\vec{r}) = [\varepsilon_r(\vec{r}) - 1]$ is called the contrast function and k_b is the wave number of the homogeneous background medium. Equation (6) is a wave equation. Using the impulse response to solve this equation in 2-D,

$$G\,(\vec{r}, \vec{r}') = \frac{-j}{4}\mathrm{H}_0^{(2)}(\mathrm{k}_b \mid \vec{r} - \vec{r}'|) \tag{7}$$

where $G\,(\vec{r}, \vec{r}')$ is also known as Green's function. $\mathrm{H}_0^{(2)}$ is the cylindrical Hankel function of the second kind of order 0. Using the impulse response, we can formulate the integral equation to solve [32],

$$\vec{E}^s(\vec{r}) = k_b^2 \int_D \left(\frac{-j}{4}\right)\mathrm{H}_0^{(2)}(\mathrm{k}_b \mid \vec{r} - \vec{r}'|)\chi(\vec{r}')E^T(\vec{r}')\, d^2r' \tag{8}$$

This is called the data equation. Here, $\vec{r}$ is at the scattered field observation locations. Data is collected by turning on one antenna (inc) and listening at all antennas (obs). So, the data is in a matrix where each column is one experiment, and each row is the data at a specific location. Each entry is a complex number representing the phase and magnitude of the scattered field.

There is another equation [18] called the state equation, which is also used for the inverse electromagnetic problem,

$$\vec{E}^T(\vec{r}) = \vec{E}^i(\vec{r}) + k_b^2 \int_D \left(\frac{-j}{4}\right) \mathrm{H}_0^{(2)}(\mathrm{k}_b \mid \vec{r} - \vec{r}' \mid) \chi(\vec{r}') E^T(\vec{r}')\, d^2 r' \tag{9}$$

In the state equation (7), $\vec{r}$ is in the domain D.

2.3 Linear Sampling Method in Inverse Scattering

As mentioned in Chapter 1, the LSM is used to determine an approximate boundary for the object. LSM combines the original data in a linear fashion to obtain combinations that result in a known scattered field at the receivers. Grid points are tested in D to see whether the points are inside or outside the object. The data collected is used to calculate a vector that represents a linear combination of experiments.

The data collected is tested using an indicator function. The linear combination of the data is represented by the equation below:

$$\sum_{n=1}^{N} \xi_n(\overrightarrow{r_p})\, E^s(\overrightarrow{r_m},\, \phi_n^i) = G_0\,(\overrightarrow{r_m}, \overrightarrow{r_p}) = \frac{-j}{4}\, H_0^{(2)}\left(k_b\left|\overrightarrow{r_m} - \overrightarrow{r_p}\right|\right) \tag{10}$$

where, $\xi_n(\overrightarrow{r_p})$ is the Herglotz kernel for sample point $\overrightarrow{r_p}$. $E^s(\overrightarrow{r_m},\, \phi_n^i)$ is the data matrix, which depends on observation location $\overrightarrow{r_m}$ and incident angle ϕ_n^i. G_0 is monopole centered at $\overrightarrow{r_p}$. In (10), $E^s(\overrightarrow{r_m},\, \phi_n^i)$ is rearranged to provide a weighted sum of the original incident fields. This rearrangement results in a scattered field that approximates a point source at $\overrightarrow{r_p}$. Equation (10) is also known as the far field equation (FFE). The circular symmetry of the scattered field is preserved due to the relationship between scattered field and the induced current. So, a circularly symmetric scattered field is produced by a circularly symmetric source centered at $\overrightarrow{r_p}$ [33]. Now, focusing in $\overrightarrow{r_p}$ of the radiating component of the induced current, the solution of (10) can be found. When $\overrightarrow{r_p}$ is outside the object, the induced current for that point will be null as $\chi(\overrightarrow{r_p}) = 0$.

The indicator function for the grid points pertains to the norm of ξ [16]. If $\| \xi \|$ is small, then $\overrightarrow{r_p}$ is within the object. As $\overrightarrow{r_p}$ approaches the boundary from the outside, $\| \xi \|$ grows without bound. Thus, each grid point can be evaluated to be inside or outside the object. This helps to provide a contour for the shape of the object.

Considering the matrix form for (10), we can write,

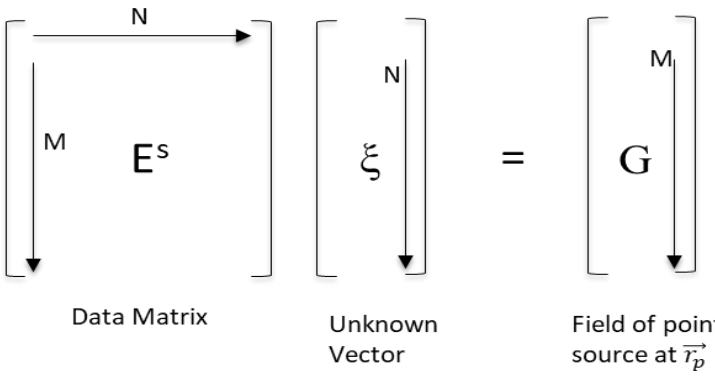

(11)

where, ξ is the N dimensional vector of unknowns, G is an M dimensional vector containing the field of point source at $\vec{r_p}$ and E^s is a NxM matrix containing the scattered field at mth receiver illuminated by the nth transmitter. Here the solution does not depend on data continuously, i.e., the problem is ill posed. Some regularization [34] is needed to avoid this ill-posedness.

2.3.1 Regularization

To solve (11), the Tikhonov-Morozov method [35]can be used. The adjoint matrix E* is used so that

$$(\alpha \boldsymbol{I} + \boldsymbol{E^*E})\,\boldsymbol{\xi} = \boldsymbol{E^*G} \tag{12}$$

where α is the regularization parameter (Tikhonov parameter) and **I** is the identity matrix. The resulting matrix equation can be solved using standard techniques, since **E*E** is a square matrix. When α = 0, the least squares solution to the problem is found.

The singular value decomposition (SVD) for matrix **E** [36] can also be used to solve (11). SVD decomposes **E** to,

$$\boldsymbol{E} = \boldsymbol{U}\,\boldsymbol{S}\,V^{H} \tag{13}$$

where the superscript 'H' indicates Hermitian-transpose. Here both **U** and $\mathbf{V}^{H}$ are unitary matrices. The matrix **S** is diagonal with real entries on the diagonal in descending order. To solve (11), substitute the singular value decomposition of **E**, and rearrange to find:

$$\boldsymbol{\xi} = \boldsymbol{V}\boldsymbol{S}^{-1}U^{H}\boldsymbol{G} \tag{14}$$

By replacing S^{-1} with:

$$\boldsymbol{S}_{nn}^{-1} = \frac{\boldsymbol{S}_{nn}}{\boldsymbol{S}_{nn}^{2} + \alpha^{2}} \tag{15}$$

The solution is regularized. And, as $\alpha \rightarrow 0$, (15) approaches $1/\mathbf{S}_{nn}$.

2.3.2 Limitations of Linear Sampling Method

LSM is often not able to reconstruct objects which are not simply connected or have a hole. It is difficult to achieve low energy solution for points which are located near the boundary but within the object. For points that are in the convex hull but outside the object, a non-negligible circularly symmetric current is also induced. So, a circular symmetry around a sampling point can be achieved even though it is outside the object. Thus LSM is

not able to always give correct information [33]. There are some extensions of LSM that have been proposed to avoid these limitations. In this thesis two of these extensions are investigated.

2.4 Generalized Linear Sampling Method (GLSM)

According to (10), a linear combination of the measured scattered fields is found where the field at the receivers matches an elementary source centered on the sampling point. This field is equivalent to the zeroth-order term of the multipole expansion of an arbitrary source. So, a possible generalization is to consider higher order multipoles for the Hankel function in (10) [37]. This will allow us to see the change of the unknown vector with changing order which will provide more information. Replacing 0 order Hankel function of (10) with G_0 to some G_n^i,

$$G_n^e(\overrightarrow{r_m},\vec{r}')=\frac{-j}{4}H_n^{(2)}(k_b\,|\,\overrightarrow{r_m}-\vec{r}'|)\,cos(n\varphi)$$
$$G_n^o(\overrightarrow{r_m},\vec{r}')=\frac{-j}{4}H_n^{(2)}(k_b\,|\,\overrightarrow{r_m}-\vec{r}'|)\,sin(n\varphi) \quad (16)$$

where the order is n and the multipole can be even (e) and odd (o). Here positive order multipole fields are considered. Scattered field has bandwidth which is related to the size of object as n=2ka where a is the size of the object. So, the maximum usable order is related to the size of the object. For n=1, equation (16) corresponds to the field radiated by two orthogonal dipole sources. The kernel of the equation is the same as the standard LSM, so all the other quantities have the same definition as (11). The Tikhonov parameter is same for all sampling points [38].

Now, the equation for the generalized LSM (also the generalized FFE) is

$$\sum_{n=1}^{N} \xi_n(\overrightarrow{r_p})\, E^s(\overrightarrow{r_m},\, \phi_n^i) = G_n^i\,(\overrightarrow{r_m}, \overrightarrow{r_p}) \tag{17}$$

The expected behavior of the regularized solution of the higher order far field equation for objects that are simple and not convex and/or not simply connected can be realized using the relation between the contrast source induced inside the scatterer J_{ind} and the contrast source corresponding to the incident field J_n^i. Applying the Schwartz inequality for the J_n^i, [37] it follows that,

$$\frac{\|J_n^i\|^2}{\|J_{ind}\|^2} \leq \|\xi_n^i\|^2 \tag{18}$$

here, $\|J_{ind}\|^2$ only depends on the original scattering experiments. So, for a given sampling point, J_n^i determines a lower bound for the energy of the regularized solution to the corresponding generalized FFE. For some given sampling point $\overrightarrow{r_p}$ and fixed (n, i), J_n^i needs to be able to radiate the field $G_n^i\,(\overrightarrow{r_m}, \overrightarrow{r_p})$ to fulfill the requirement for generalized FFE.

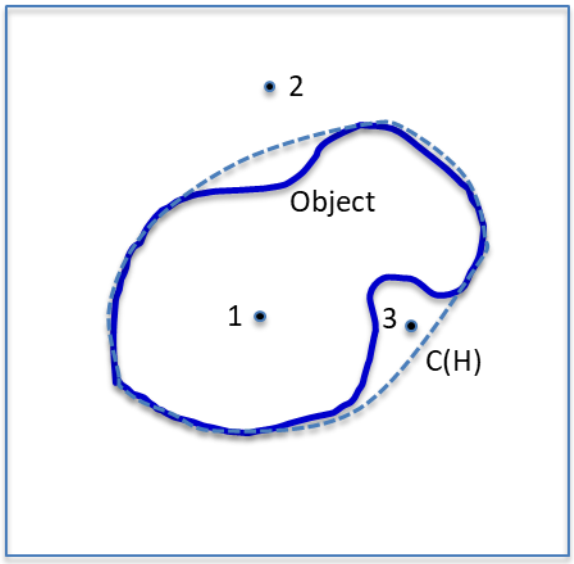

Figure 2-2 A typical non-convex object; solid line, object; dashed line, convex hull

Now consider the generic object with C(H) as the convex hull that encloses it as shown in Figure 3.1. For points that are inside the object, such as point 1, the value of $\left\|\xi_n^i\right\|^2$ would be small, indicating that the point is inside the object. For point 2, the value of $\left\|\xi_n^i\right\|^2$ would be large, indicating that the point is outside the object.

Consider points that are inside the convex hull but outside the object, such as point 3. The equivalence principle indicates that it is possible to induce a source J_n^i. This point is capable to radiate the required field $G_n^i\left(\overrightarrow{r_m}, \overrightarrow{r_p}\right)$ which is similar to point 1. Thus it would indicate that the point is inside the object although it is outside the object. The overall result would be the convex hull of the object rather than the actual shape of the object. This is the reason why LSM fails to retrieve the information for the not connected and not convex objects. The corresponding contrast source J_n^i will provide a spatial behavior due to the corresponding multipolar field when it satisfies (18). This field has specific angular behavior with respect to the sampling point. So J_n^i will exhibit similar behavior over the

object. Based on this property, the energy solution will attain low values for points that are inside the object.

For n>0, it corresponds to the increasingly fast angular oscillations centered around the sampling point. It is difficult to achieve low energy solution for those points which are located near the boundary but within the object [33]. Consider points that are inside the convex hull but do not belong to the object. Here, contrast sources which support multipolar fields can also be induced. It happens as long as there is enough space to allocate a multipolar source. So, both standard and higher order indicator may have low values for those points. To solve this problem another indicator function is proposed [37].

$$I_p = \prod_{n=1}^{p} \frac{\|\xi_0\|^2}{\|\xi_n^e\|^2} \frac{\|\xi_0\|^2}{\|\xi_n^o\|^2} \tag{19}$$

where I_p is the indicator for poles up to order P and P=2ka. It is possible to show that one or more $\left\|\xi_n^i\right\|^2$ will have smaller values than the zeroth order indicator $\|\xi_0\|^2$. This typically occurs for points that are outside the object and inside the convex hull. This will yield a large value for the indicator. Therefore, points in the convex hull and outside the object may have a large I_p. This indicator may be able to detect a hole or concavities inside the object.

2.5 Multipole based Linear Sampling Method (MLSM)

The above approaches to develop LSM method are based on the mathematical perspective. The multipole based LSM (MLSM) is based on the physical perspective as it refers to the multipole expansion of the scattered field [39]. It uses a physical regularization for the reconstruction of the scatterer. It is possible to have a large number of multipoles for the scattered field expansion, depending on the object. This method uses only the monopole and dipole terms for the reconstruction. All higher order poles are ignored. Thus, a physical approximation is used rather than a mathematical regularization.

MLSM has convenience over the other methods in the following aspects: it provides a physically grounded regularization rather than a mathematical regularization. So, it is beneficial to understand LSM in terms of scattering physics. MLSM is easy to implement and provides better reconstruction for objects that are not simply connected. It is easy to select the maximum multipole order rather than the regularization parameter as in traditional LSM. MLSM also provides a link to other imaging methods such as the suppression of secondary sources induced at other point-like scatterers in MUSIC imaging [40].

MLSM is a multipole expansion of the data matrix. For each sample point $\vec{r}_p$,

$$E_s\left(\overrightarrow{r_m},\ \phi_n^i\right) = \sum_l \alpha_l\left(\overrightarrow{r_p},\ \phi_n^i\right) H_l^{(2)}\left(k_b \left| \overrightarrow{r_m} - \vec{r}_p \right|\right) e^{jl\, Arg\left(\overrightarrow{r_m} - \vec{r}_p\right)} \tag{20}$$

here, $H_l^{(2)}\,(k_b\,|\overrightarrow{r_m}-\vec{r}_p|)e^{jl\,Arg(\overrightarrow{r_m}-\vec{r}_p)}$ represents the multipole radiation functions that are all centered at $\vec{r}_p$. $Arg\left(\overrightarrow{r_m}-\vec{r}_p\right)$ is the angle between far-field observation point $\overrightarrow{r_m}$ and sample point $\vec{r}_p$. Here multipole coefficients are determined for order l=−L, −L+1, …0, 1, 2, …L. The number of multipoles is 2L+1. $\alpha_l(\overrightarrow{r_p},\,\phi_n^i)$ are the multipole coefficients that form a new matrix **A**. Now applying LSM with the new matrix, we find linear combination of experiments, so that all the multipoles cancel and only monopole terms exist. This is repeated for every $\vec{r}_p$.

Considering a system of N transmitter and M receiver, for each incidence n (20) can be written as,

$$\boldsymbol{E}=\boldsymbol{HA} \tag{21}$$

where, $\boldsymbol{E}$ is an N dimensional vector and contains the receiver measurements. $\boldsymbol{H}$ is a matrix of dimension M× (2L+1) and contains the multipole radiation terms of (20). $\boldsymbol{A}$ is a 2L+1 dimensional vector that consists of effective multipole coefficients $\alpha_l\left(\overrightarrow{r_p},\,\phi_n^i\right)$.

Using the least squares pseudoinverse the value of $\boldsymbol{A}$ can be determined uniquely. Similar to the fundamental equation of LSM (11), the discretized version for N experiments is:

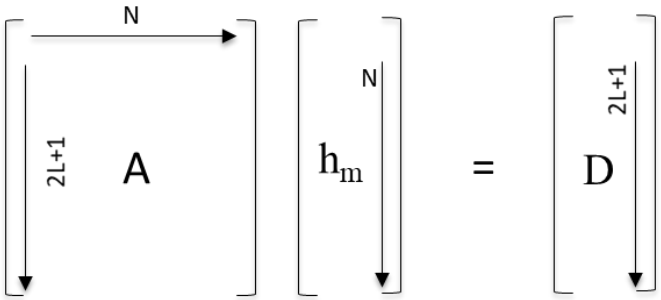

(22)

here, $h_m$is an N dimensional vector that needs to be determined. **D** is a vector that has all the elements except the (L+1)th element as zero. The (L+1) th element refers to the monopole term. The value of h_m can be resolved from (22) by pseudoinverse. It depends upon the number of multipoles considered. However, the value of h_m is similar for both MLSM and LSM when the value of L is very large. It suggests that the multipoles of higher order than the considered (2L+1) multipoles have very less and diminishing contribution to the scattered field. Also, large number of multipoles increases the computational complexities. However, at least (2L+1) receivers are needed to solve (21).

In [39] it is suggested to use L=1 for reconstruction. The use of L=1 implies that solving (21) to get an optimal combination of the monopole and dipole current such that the scattered field is matched with the radiation fields as closely as possible. By solving (22), h_m is determined such that the contribution of the dipole current is very low. Thus, the reduction of requirement of h_m will suppress the contribution from all other higher order multipoles. In most cases the monopole and dipole have the dominance on higher order but there are scatterers where the higher order multipole will be dominant. In those cases the choice of higher value of L needs to be considered.

The indicator function for MLSM is:

$$I_m = -\log_{10}(||h_m||/||h_m||_{max}) \tag{23}$$

here, I_m is in dB scale and it begins at 0 and grows. $||h_m||$ is computed for each grid point and maximum norm is found over the domain. Then, I_m is graphed. Usually a contour is used to indicate “inside” vs “outside” points.

3. RESULTS AND DISCUSSION

3.1 Introduction

In this section the simulated results of the presented methods are shown and discussed. MEEP software [41] is used to generate the electromagnetic fields data. Then the inhouse software is used to generate the data matrix and regularize the data. GNU plot has been used to plot the results. The data matrix consists of the scattered fields for the sampling points. The antennas are placed an equal distance from each other and 2λ from the center of the domain as shown in Figure 2.1. The scattered fields are measured for each incident angle. The columns of the data matrix consist of these scattered fields. So, the number of columns is the number of incident points and the number of rows is the number of observation points. Then the right side of the FFE (11) is computed as the field of a point source. The unknown vector ξ is determined to match the right side. The norm of $||\xi||$ helps to determine the boundary of the object. Here, 10% noise has been added to the data.

The goal is to reconstruct the boundary of the object from the scattered field data. The reconstruction of the object shape depends on different parameters such as the relative permittivity, size, shape, number of observation and incident points. In this thesis the effect of these parameters has been investigated. The result for the LSM, GLSM and MLSM have been presented and a comparison is discussed briefly in this chapter. Each method is evaluated according to how well the boundary is reconstructed.

3.2 Linear Sampling Method Results

As discussed in the previous chapter, LSM can give a satisfactory reconstruction for the simply connected objects but may not for concave or not convex objects. The induced currents are focused around the sampling points for the simply connected objects. Also, these induced currents are different from zero due to the induced regularization. It identifies whether the points are inside or outside of the object. This helps to determine the boundary of the object. The boundary of the object is determined by using the norm of $||\xi||$ from (11).

Figure 3.1 shows the reconstruction of the elliptical object using the LSM. The length of the object is $a=0.5\lambda$, width is $b=0.25\lambda$ and relative permittivity is $\varepsilon_R=3.0$. It is a simply connected object and from the result it is evident that LSM can retrieve the approximate shape. It is also shown that using a greater number of observation and incident points helps to obtain the better result. The reconstruction of image in Figure 3.1 (b) and (c) is better than (a). But there is a point where increasing the number of observation and incident points does not help that much also there is a practical limitation using a greater number of antennas.

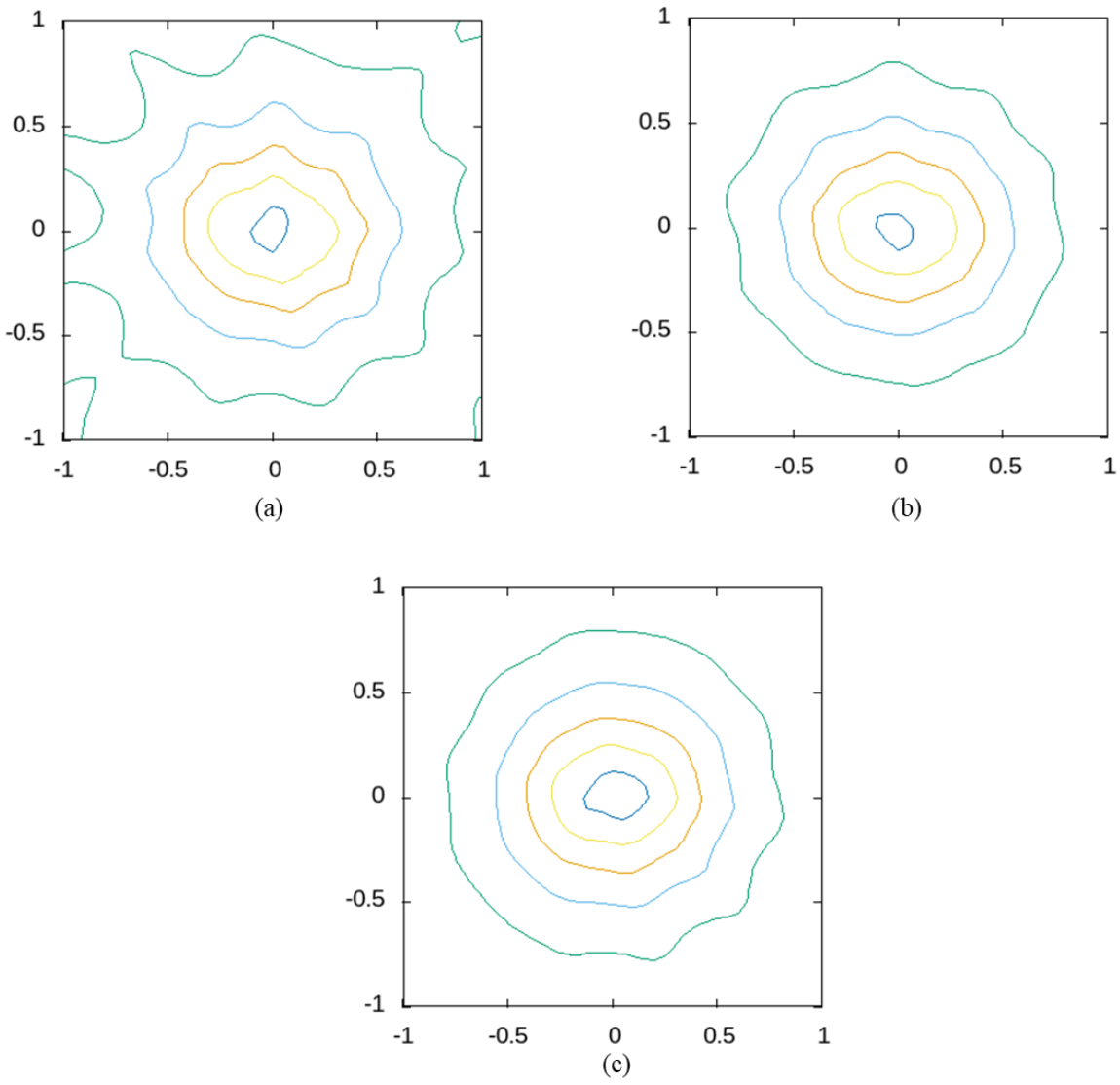

Figure 3-1 Reconstruction of elliptical object using number of observation and incident (a) 12 points, (b) 24 points, (c) 48 points (using contour value from 0.1 to 1000)

LSM has been used for other objects that are not simply connected or have a hole inside. In these cases, LSM can only retrieve the convex hull rather than the actual shape of the object. The reconstruction results for the thick U, circular ring and S-shaped object are shown in Figure 3-2. All the objects have relative permittivity ε_R=2.0. The number of incident and observation points is 19 evenly spaced on a circle of radius 2λ. The proposed interpretation for such object is explained by (10). Considering a point between the arms

of thick U object of Figure 3-2(a), a current can be induced which is approximately circularly symmetric around the sampling point. It radiates a field that matches the right-hand side of the FFE. As a result, the point is erroneously detected as belonging to the object. However no focusing or circular symmetry is possible for the points apart from the concavity. So, the convex envelope of the object shown in Figure 3-2 (d) is retrieved. This happens for the ring and the S-shaped objects as shown in Figure 3-2 (e), (f).

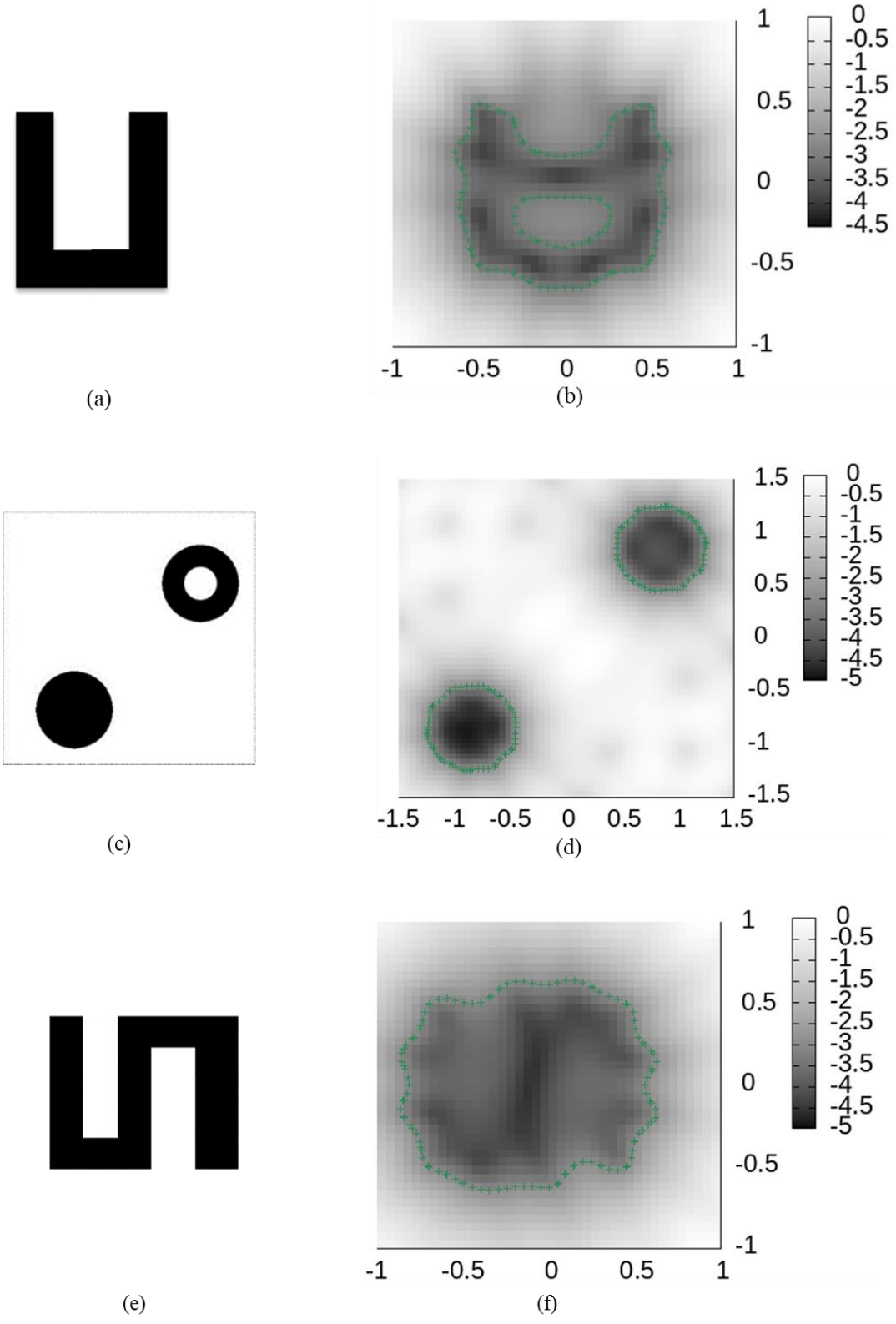

Figure 3-2 Concave objects (a) thick U, (c) circular and ring, (e) S-shape object; reconstructed image using LSM (b) thick U, (d) circular and ring, (f) S-shape object;

The solution of (10) is highly dependent on the relative permittivity ε_R. The change of ε_R affects the contrast function, thus the solution of the problem. The electromagnetic field is forced to interact several times with the object before being detected when the relative permittivity is high. This results in LSM being insufficient to estimate the object structure. Figure 3-3 shows the change of reconstruction with the change in permittivity. The reconstruction gets worse for thick U object with higher relative permittivity.

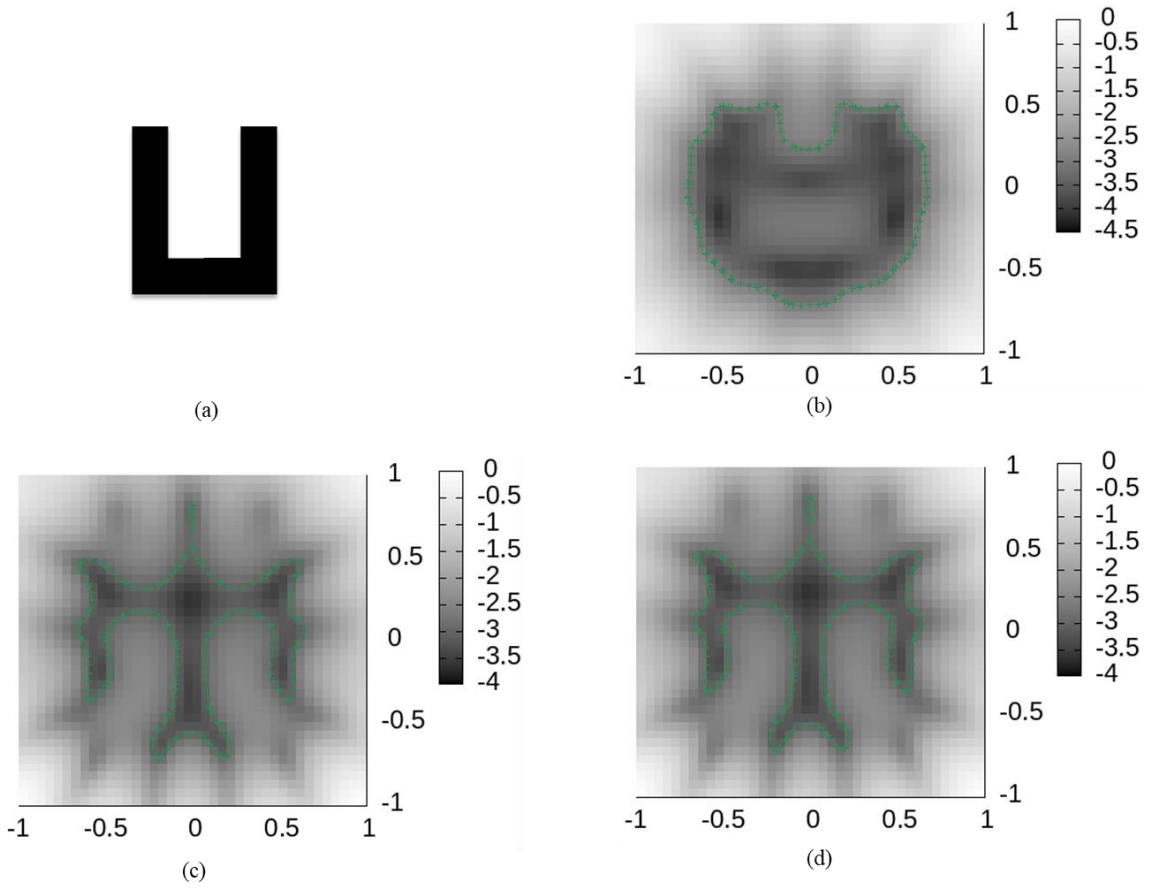

Figure 3-3 Changes of LSM results with changing ε_R for thick U object (a)target object with (b) ε_R=3, (c) ε_R=4, (d) ε_R=6

This problem can be avoided by increasing the regularization parameter α. Figure 3-4 shows that changing the values for α helps the reconstruction even with the fundamental LSM. The thick U object with ε_R =2 or 3 has been used here and the value for α is 0.05 in Figure 3-4 (a) and 0.5 in Figure 3-4 (b). The resultant shape is similar to the original one with some discrepancies between the arms of the object. However the results are better than the expected one with the higher permittivity. The problem is that one must use the correct regularization parameter to get good results.

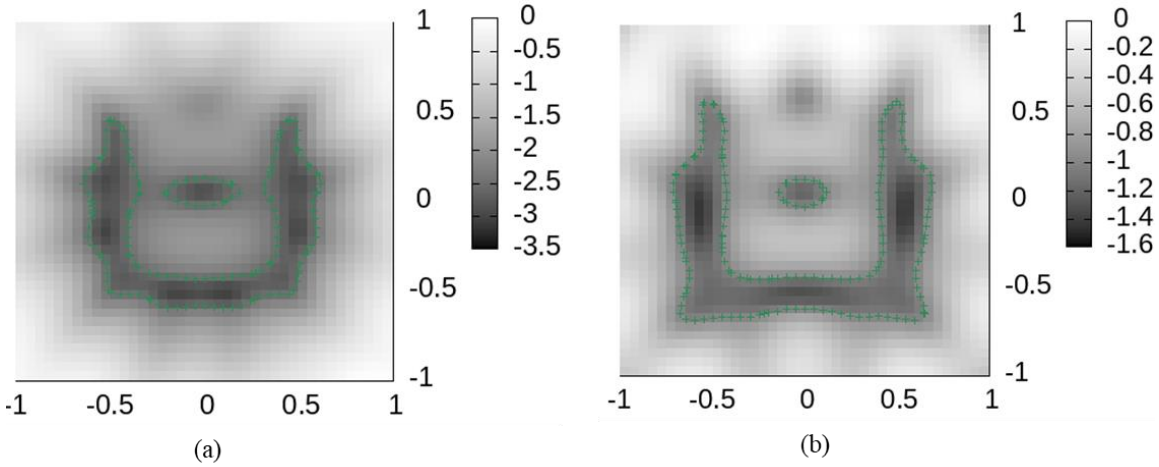

Figure 3-4 Reconstruction with LSM with higher α for thick U object (a) ε_R=2, α=0.05; (b) ε_R=3, α=0.5

The simulated results for standard LSM suggest that LSM can reconstruct the boundary of simply connected objects. It fails to reconstruct the boundary when the object is concave or has a hole in it. Although it can retrieve the convex hull of the object. However, it is interesting to see the effect of regularization parameter for such objects. The reconstruction gets better with the use of proper regularization parameter.

3.3 Generalized LSM Results

The GLSM uses the higher order Hankel functions. The highest order that can be used is limited by the size of the object. It is interesting to look at how minimum of $\|\boldsymbol{\xi}\|$ varies with the order of the Hankel function. Figure 3-5 shows the change of minimum $\|\boldsymbol{\xi}\|$ with the change of n. The change has been shown for two elliptical objects with a=0.5λ and a=1.5λ. Figure 3-5(a) shows that both the positive and negative higher order show similar behavior for minimum of $\|\boldsymbol{\xi}\|$. Figure 3-5(b) shows that increasing the size of the object allows the use of higher order Hankel functions. For the lower values of n the change of minimum $\|\boldsymbol{\xi}\|$ all over the grid points is small. But as the order increases the minimum of $\|\boldsymbol{\xi}\|$ grows. The maximum usable order for a = 0.5λ is 2 and for a=1.5λ is 6. The small values of minimum $\|\boldsymbol{\xi}\|$ can also be used to estimate the scattered field bandwidth.

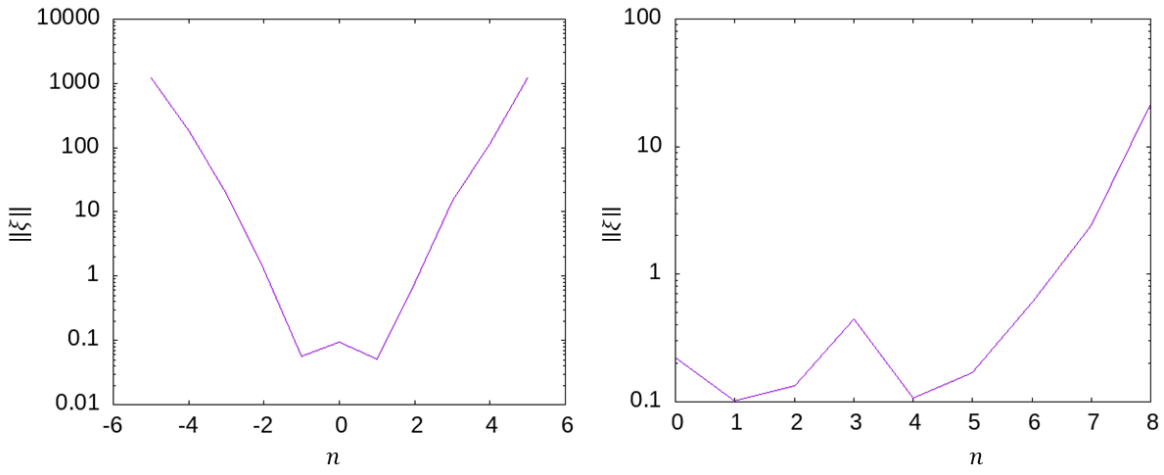

Figure 3-5 Change of minimum $\|\xi\|$ with changing of value of n (a) n=-6 to +6 for object with a=0.5 λ ; (b) n=0 to +8 for object with a=1.5

The scattered field bandwidth can be estimated as 2ka where a is the maximum dimension of the object. Table 3.1 shows the comparison of scattered field bandwidth and the maximum usable order (n_{max}). For each elliptical cross section a, the estimated bandwidth and the maximum usable order n_{max} are listed. Also, the ratio of bandwidth to maximum order is relatively consistent at 3. Therefore, it is suggested that the maximum order can be used to estimate the bandwidth of the scattered field.

Table 2.1 Comparison of scattered field bandwidth and the maximum usable order (n_{max}).

a	2ka	n_{max}	2ka/ n_{max}
0.5	6.28	2	3.14
1.0	12.26	4	3.07
1.5	18.85	6	3.14

Figure 3-6 shows the result of the reconstructed images for elliptical object with a=0.5λ. It is interesting to note that the reconstructed boundary gets smaller with the increased order, but it is still reconstructible as long as it matches the condition of 2ka. As a result, Figure 3-6(c) shows that the boundary is no longer reconstructible for order n=4.

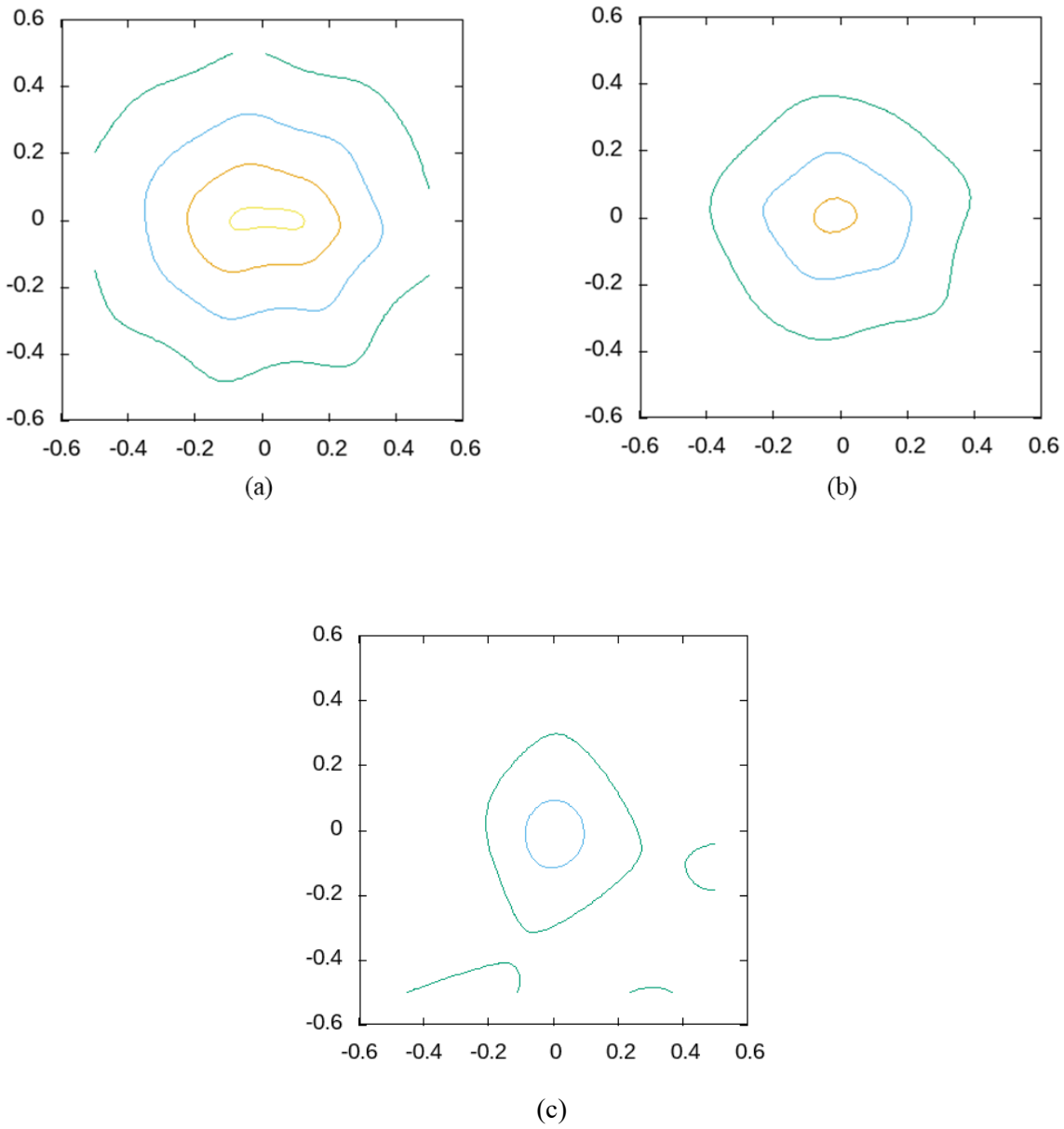

Figure 3-6 Change of boundary for elliptical object of length a=0.5λ and width b=0.25λ with value of (a) n=1, (b) n=2 (c) n=4 (using contour value 0.1 to 1000)

As discussed in section 2.4, GLSM cannot retrieve the correct information for points that are close to the boundary. So, another indicator function (19) for GLSM is proposed. This is applied for objects that are used in Figure 3-2. The results are shown in Figure 3-7. The indicator function gives correct information for points that are inside the

convex hull but outside the object. As shown in section 3.2, LSM cannot retrieve the shape for the thick U object as it fails to detect the points that are inside the two arms but outside the object. Conversely, using the indicator of (19) the shape is retrieved almost properly with the value I_6. It clearly reveals the concave shape.

This is also applied to the circular and ring shape object. As shown in Figure 3.2, the standard LSM cannot differentiate the two figures as it cannot account for their different inner features. However, the new GLSM indicator function correctly retrieves the two objects. The indicator I_4 allows to see the hole inside the ring object. It shows values in the hole of the ring that are comparable to the background medium. Thus, it can detect the hole inside the object.

For S-shape object the reconstruction with the indicator I_7 is better than the standard LSM. But it is not as good as the other objects shown before. The middle part of the S-shaped object shown in Figure 3-7 (c) is still not reconstructible by GLSM. This is due to the higher reflections of the object and the lack of circular symmetry in the induced current. However, there is significant improvement with this approach.

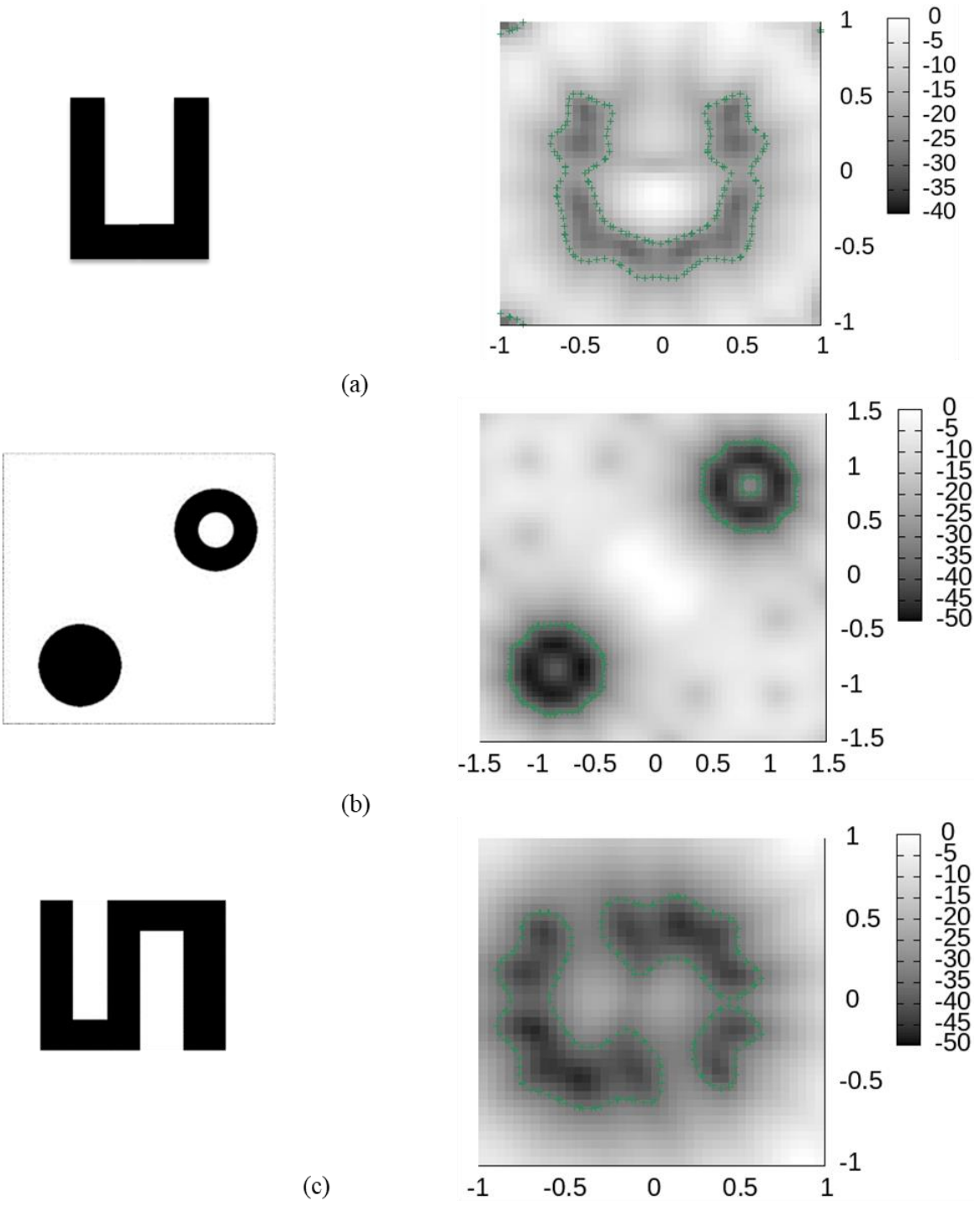

Figure 3-7 Reconstruction using GLSM (a) thick U for I_6, (b) circular and ring shape for I_6, (c) S-shape for I_7

There is another problem with the GLSM method. The selection of the boundary contour is not fixed for all the objects. This is an issue when GLSM applied to an arbitrary object. In this thesis the contour used for GLSM is different for each object depending on the actual size of the object to get a better view of the reconstructed image. This is not feasible for practical application when the object is unknown.

Similar to the result of LSM, the result of GLSM also depends on the relative permittivity of the object. Figure 3-8 shows how the increment of ε_R affects the reconstruction for the thick U object. For the values of ε_R=4 or 6 the boundary is no longer achieved.

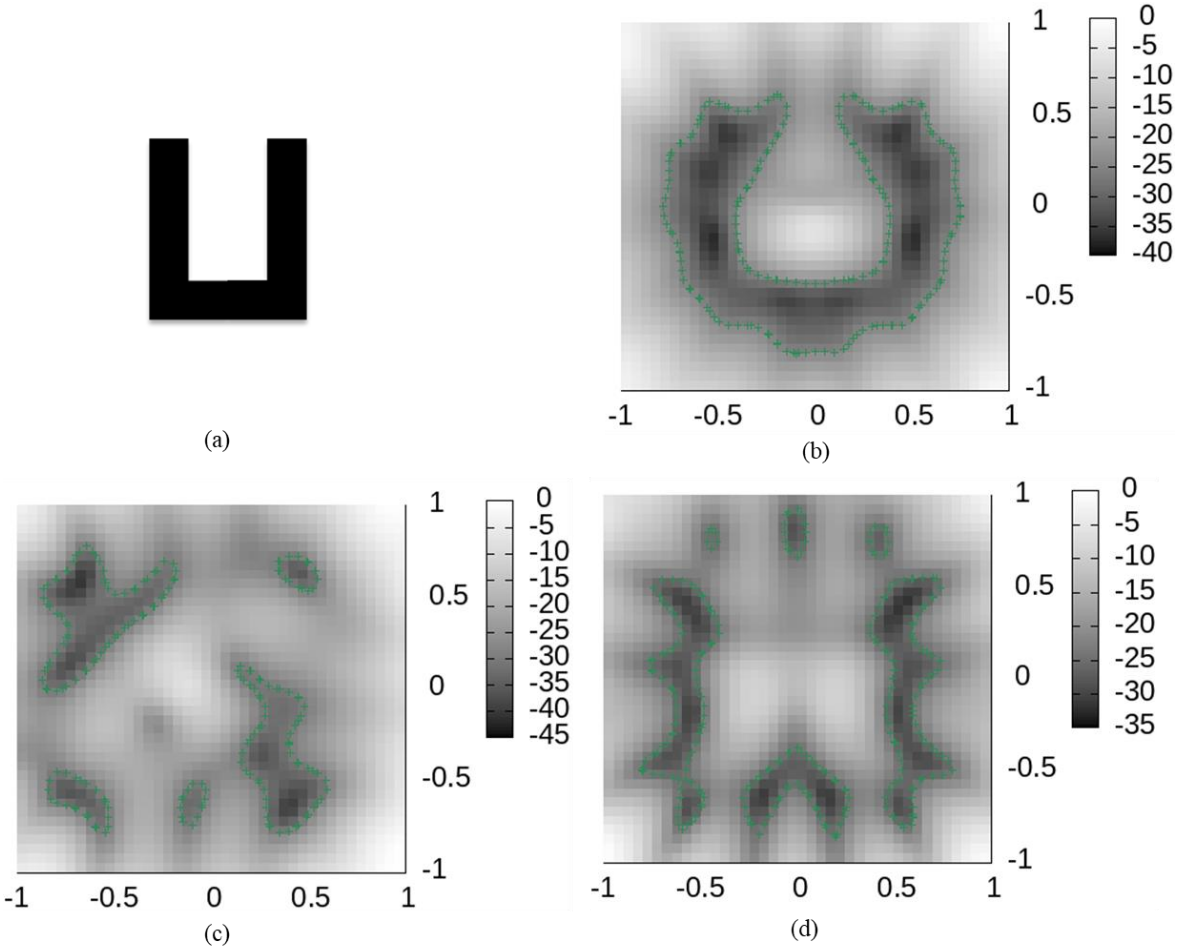

Figure 3-8 Changes of GLSM results with changes of ε_R of thick U (a) ε_R=3, (b) ε_R=4, (c) ε_R=6

This problem can be solved with the use of proper regularization parameter. With a change of α, the boundary of the object can be achieved. Figure 3-9 shows that with the value of α=0.05 the reconstruction for the thick U object with GLSM indicator I_6 gives better result than with α=0.01. This will allow better reconstruction even with higher relative permittivity.

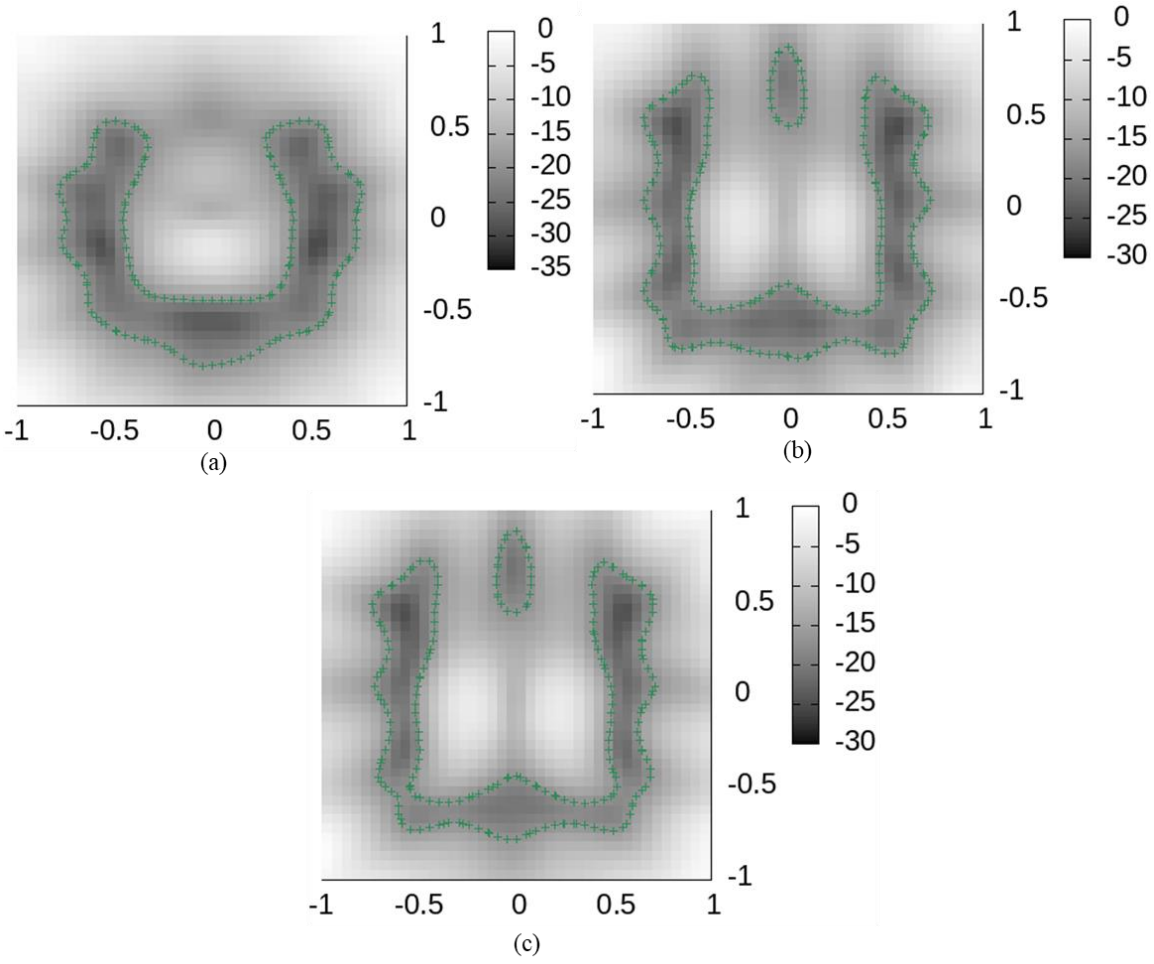

Figure 3-9 GLSM results for thick U for higher regularization parameter α=.05 (a) ε_R=3, (b) ε_R=4, (c) ε_R=6

So, GLSM can reconstruct the boundary of objects which are not simply connected. Also, changing the regularization parameter helps the reconstruction when the relative permittivity is high. However, GLSM fails for the S-shaped object.

3.4 Multipole based LSM Results

The MLSM is based on physical regularization rather than using the regularization parameter. As discussed in Section 2.5, L=1 has been used for the reconstruction from the solution of (20). This allows to use the combination of monopole and dipole currents such that the scattered field matches the resultant radiation field as closely as possible. The result using MLSM with L=1 for the thick U, circular and ring object and S shape object with ε_R=2 is shown in Figure 3-10. There is no added noise in this section. The additional noise does not affect the results for MLSM. From Figure 3-10(a) and (b), it can be noticed that MLSM can retrieve the shape of the object almost the same as the GLSM but there are some discrepancies for the ring object. For the S-shape object, the reconstruction is much better than GLSM and LSM. In MLSM, the multipole expansion of the scattered field only uses the dominant poles. Here the dominant poles are monopole and dipole. There can be cases where the dominant poles are different. In such cases the value of L will need to be higher.

Another advantage of using MLSM is the threshold used to estimate the scatterer support. Previously, the threshold was different for different objects. So, one needs to have some idea about the shape of the scatterer to determine the threshold. This problem can be avoided by using the MLSM. Here, the threshold is 0.8 of the maximum of h_m. This has been used for all types of scatterers and the results shows a better approximation than the previous methods.

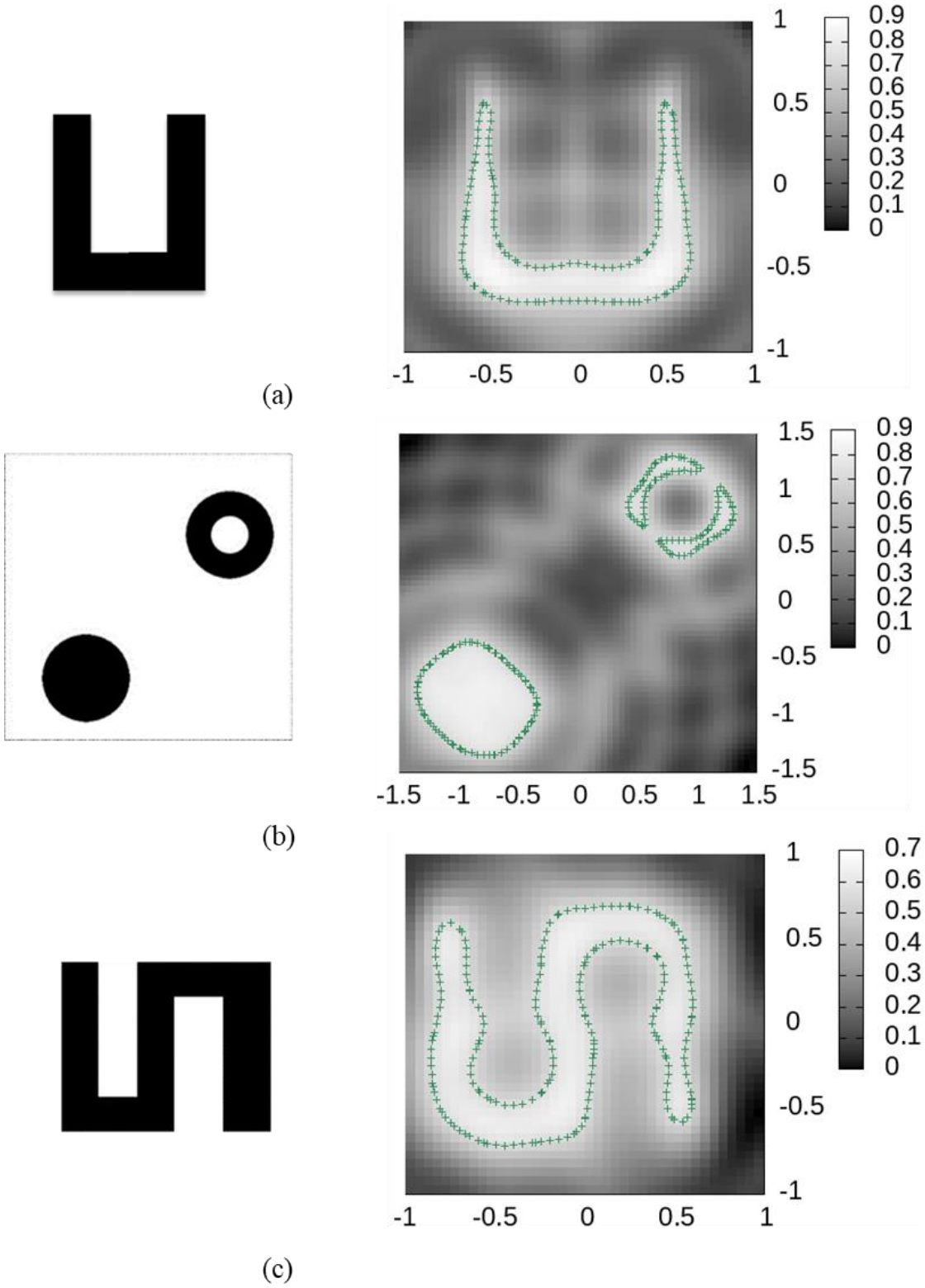

Figure 3-10 MLSM results with L=1 for (a) thick U, (b) circular and ring, (c) S-shape object

The change of relative permittivity also affects the results of MLSM. With the increment of ε_R the reconstruction gets worse for the object. The effect of changing ε_R is shown in Figure 3-11 for thick U object. It is evident that multiple interactions of fields with the object affects the reconstruction. Figure 3-11 (b) and (c) shows that higher values of ε_R= 4 or 6 disrupt the reconstruction. The shape of the object is no longer similar to the original one. This problem cannot be avoided with the higher regularization parameter as mathematical regularization is not applied in MLSM.

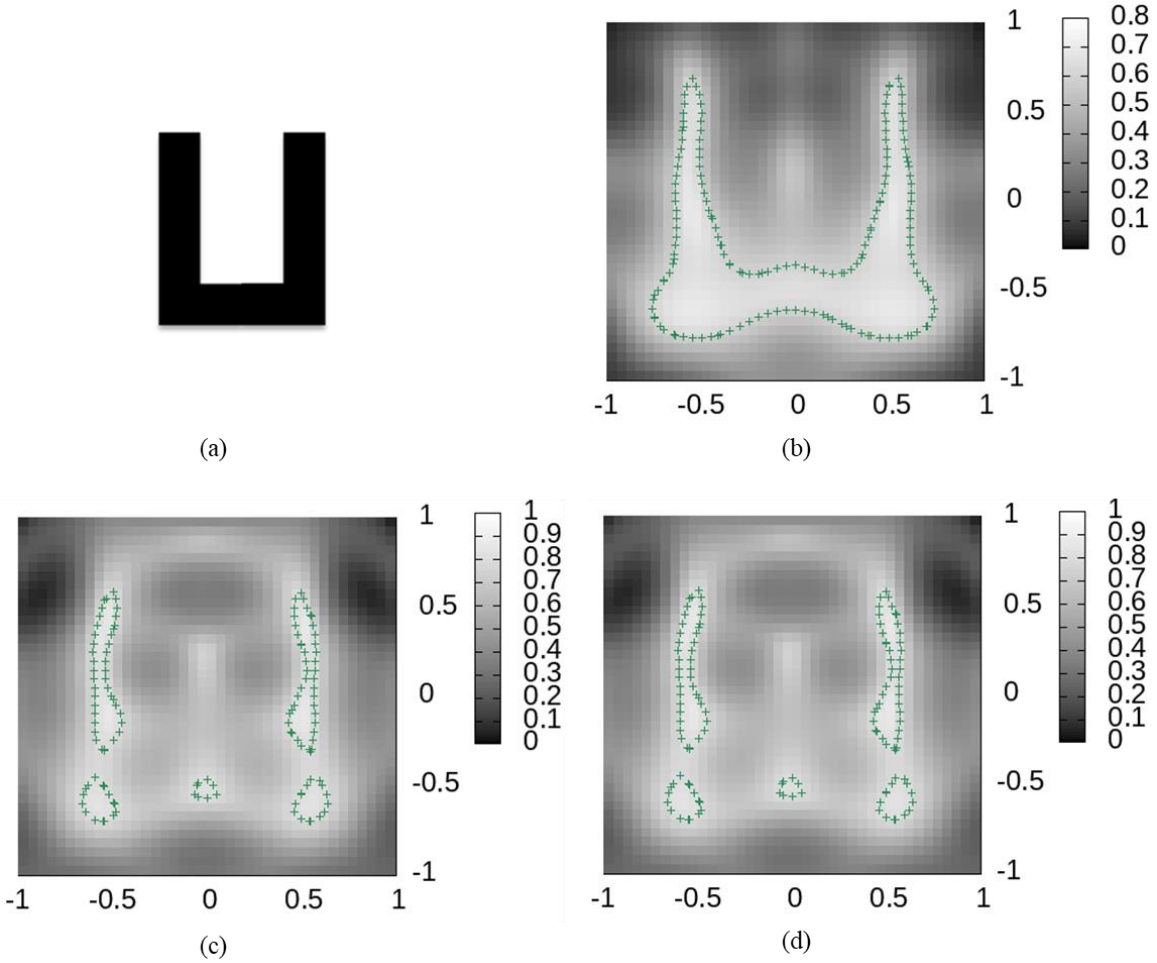

Figure 3-11 Changes of MLSM results with changes of ε_R of (a) thick U object (b) ε_R=3, (c) ε_R=4, (d) ε_R=6

From the above simulated result it is evident that MLSM can reconstruct the boundary successfully for different shapes of objects. The advantage of this method is the constant value of boundary contour. However, the higher permittivity affects the reconstruction severely. Using the higher order poles does not help to avoid this problem. Some simulations were done with higher order poles in case of high permittivity, but it did not show better reconstruction.

4. SUMMARY, CONCLUSIONS AND FUTURE WORK

4.1 Summary

The objective of this work is to investigate the extensions of LSM for the reconstruction of the shape of unknown object. The formulation of LSM has been discussed briefly to solve the inverse scattering problem. LSM allows determination of the support of unknown scatterer. However, LSM fails to reconstruct the actual shape when the object is not simply connected or has a hole. LSM cannot retrieve correct information for points that are inside the convex hull but outside the object. Thus, the convex hull of the object is retrieved rather than the actual shape. Some extensions of LSM have been proposed to avoid this problem. In this thesis, two of the extensions: GLSM and MLSM, are discussed and the results are compared.

Generalized LSM is based on using higher order of the Hankel function in the right side of FFE and what kind of information the change brings. Furthermore, the post processing scheme has been used to combine and take advantage of the huge amount of information hidden in the solution of FFE for different orders. Such an approach overcomes the limitations of standard LSM. The indicator used for GLSM is a reliable imaging tool. It can retrieve the correct information for concave objects where standard LSM fails. So, it improves the overall reconstruction capabilities. However, it does not work well for some complex shaped objects like the S-shape object.

Multipole based LSM uses a physical regularization rather than the mathematical regularization used in LSM and GLSM. The multipole expansion of the scattered field is

studied rather than studying the circular symmetry of the induced current. In this thesis only monopole and dipole terms are used, and all other higher orders are truncated. This approach shows better reconstruction than the standard LSM and GLSM. The physical approximation used here is very different from the Tikhonov regularization, but it performs better even for the complex scatterer like S-shape object. Another advantage of the MLSM is that it uses a constant boundary contour for all objects. The boundary contour requirement is varied with the size of the object in GLSM and standard LSM.

The permittivity of the object affects the solution of the FFE. Thus, the reconstruction gets worse for all the methods with higher relative permittivity. In GLSM and standard LSM, this problem can be avoided by using larger value for the regularization parameter. However, it is difficult to choose the correct value of the parameter. MLSM does not use the regularization parameter, so this problem persists for MLSM reconstruction.

4.2 Conclusion

In this thesis, the extensions of LSM have been studied and compared to identify which method works better to reconstruct the shape of different types of scatterers. The solution of inverse scattering problem using LSM helps to reconstruct the boundary of the object. LSM can be used in different situations like subsurface or near field imaging, provided that focusing of the induced currents can be formulated. LSM works well for simply connected objects but fails for complex objects. Thus, some extensions have been proposed which work with complex objects. This investigation of GLSM and MLSM helps to identify the comparisons between these methods.

GLSM combines the huge information of the FFE for different orders with a post-processing scheme to get better results than LSM. The expectation is fulfilled nicely except for some complex shaped objects. The study of MLSM shows that the physical approximation of the scattered field gives better results than GLSM. Using the multipole expansion of the scattered field demonstrates good performance for various complicated scatterers. However, the effect of higher relative permittivity still is a problem for MLSM.

4.3 Future Work

In this thesis three methods are presented to solve the inverse scattering problem. All these solutions are done for two-dimensional imaging. The good performance and extreme computational efficiency of LSM makes it attractive in three-dimensional imaging [28].

The combined indicator in GLSM shows overall improvement of the reconstruction process. This is relevant for hybrid approaches also. The reconstruction capabilities of a Quantitative approach can be improved by exploiting the result of qualitative methods such as GLSM [18], [26]. So, the results of GLSM can be used as a priori information to implement a quantitative method.

The effect of the regularization parameter has been investigated for GLSM. It shows that higher value of the regularization parameter helps the reconstruction of objects with higher permittivity. Further investigation can be done to choose appropriate value of the regularization parameter.

MLSM introduces a physical explanation of LSM. Two-dimensional scatterers have been considered in this thesis. The next step can be to develop MLSM for three-

dimensional imaging. In this case the fundamental radiating source is dipole instead of monopole. So, necessary step should be considered in the extension of MLSM with dipole radiating source. As MLSM is based on the physical approximation, it will lead to wider applications of LSM. The better reconstruction of the object suggests that it can be useful to the through-wall-imaging [38]. In through-wall-imaging there is great variability in both adopted materials and the internal structures of a wall. MLSM can be used to detect this variability and give a better reconstruction of the target.

REFERENCES

[1] M. Pastorino and A. Randazzo, “Microwave Imaging Methods and Applications,” *Artech House*, 2018.

[2] Radar Systems Electronic Systems Society, “IEEE Standard Letter Designations for Radar-Frequency Bands,” *IEEE Std 521-2002 (Revision IEEE Std 521-1984)*, vol. 1984, pp. 0_1-3, 2003.

[3] ITU, “Nomenclature of the frequency and wavelengh bands used in telecommunications V Series Vocabulary and related subjects,” *ITU-R Recomm. Reports, ITU-R V.431-8*, vol. 8, p. 5, 2015, [Online]. Available: http://www.itu.int/ITU-R/go/patents/en.

[4] S. O. Nelson, “Dielectric spectroscopy in agriculture,” *J. Non. Cryst. Solids*, vol. 351, no. 33-36 SPEC. ISS., pp. 2940–2944, 2005, doi: 10.1016/j.jnoncrysol.2005.04.081.

[5] S. Trabelsi and S. O. Nelson, “Nondestructive sensing of physical properties of granular materials by microwave permittivity measurement,” *IEEE Trans. Instrum. Meas.*, vol. 55, no. 3, pp. 953–963, 2006, doi: 10.1109/TIM.2006.873787.

[6] S. O. Nelson, “Dielectric spectroscopy of fresh fruit and vegetable tissues,” *ASAE Annu. Int. Meet. 2004*, no. February 2005, pp. 3607–3626, 2004, doi: 10.13031/2013.16693.

[7] D. El Khaled, N. Novas, J. A. Gazquez, R. M. Garcia, and F. Manzano-Agugliaro, *Fruit and vegetable quality assessment via dielectric sensing*, June 2015,Sensors 15(7):15363-15397, DOI:10.3390/s150715363vol. 15, no. 7..

[8] H. Jawad *et al.*, “Microwave modeling and experiments for non destructive control

improved quality of fruit," *2017 IEEE Conf. Antenna Meas. Appl. CAMA 2017*, vol. 2018-January, pp. 124–127, 2018, doi: 10.1109/CAMA.2017.8273375.

[9] L. E. Larsen and J. H. Jacobi, *Medical Applications of Microwave Imaging*. IEEE Press, New York, USA, 1986.

[10] E. Zastrow, S. K. Davis, M. Lazebnik, F. Kelcz, B. D. V. Veen, and S. C. Hagness, "Development of anatomically realistic numerical breast phantoms with accurate dielectric properties for modeling microwave interactions with the human breast," *IEEE Trans. Biomed. Eng.*, vol. 55, no. 12, pp. 2792–2800, 2008, doi: 10.1109/TBME.2008.2002130.

[11] L. M. Neira, R. O. Mays, and S. C. Hagness, "Human Breast Phantoms: Test Beds for the Development of Microwave Diagnostic and Therapeutic Technologies," *IEEE Pulse*, vol. 8, no. 4, pp. 66–70, 2017, doi: 10.1109/MPUL.2017.2701489.

[12] N. K. Nikolova, "Microwave imaging for breast cancer," *IEEE Microw. Mag.*, vol. 12, no. 7, pp. 78–94, 2011, doi: 10.1109/MMM.2011.942702.

[13] E. C. Fear, P. M. Meaney, and M. A. Stuchly, "Microwaves for breast cancer detection?," *IEEE Potentials*, vol. 22, no. 1, pp. 12–18, 2003, doi: 10.1109/MP.2003.1180933.

[14] S. Al Muqatash, M. Khamechi, and A. Sabouni, "Detection of the cervical spondylotic myelopathy using noninvasive microwave imaging technique," *2017 IEEE Antennas Propag. Soc. Int. Symp. Proc.*, vol. 2017-January, pp. 783–784, 2017, doi: 10.1109/APUSNCURSINRSM.2017.8072434.

[15] M. G. Amin and F. Ahmad, *Through-the-Wall Radar Imaging: Theory and Applications*, vol. 2. Elsevier Masson SAS, 2014.

[16] H. H. and M. P. David Colton, “The linear sampling method in inverse electromagnetic scattering theory,” *Appl. Numer. Math.*, p. Volume 62, Issue 6, Pages 699-708, 2012.

[17] J. H. Richmond, “Scattering by a Dielectric Cylinder of Arbitrary Cross Section Shape,” *IEEE Trans. Antennas Propag.*, vol. AP-13, no. 3, pp. 334–341, 1965, doi: 10.1109/TAP.1965.1138427.

[18] L. Crocco, I. Catapano, L. Di Donato, and T. Isernia, “The linear sampling method as a way to quantitative inverse scattering,” *IEEE Trans. Antennas Propag.*, vol. 60, no. 4, pp. 1844–1853, 2012, doi: 10.1109/TAP.2012.2186250.

[19] F. Cakoni and D. Colton, *Qualitative Methods in Inverse Scattering Theory*. Springer Science & Business Media, 2005.

[20] W. C. Chew and Y. M. Wang, “Reconstruction of Two-Dimensional Permittivity Distribution Using the Distorted Born Iterative Method,” *IEEE Trans. Med. Imaging*, vol. 9, no. 2, pp. 218–225, 1990, doi: 10.1109/42.56334.

[21] X. Chen, Y. U. Zhong, and K. Agarwal, “Subspace methods for solving electromagnetic inverse scattering problems,” METHODS AND APPLICATIONS OF ANALYSIS, vol. 17, no. 4, pp. 407–432, 2011.

[22] L. Souriau, B. Duchêne, D. Lesselier, and R. E. Kleinman, “Modified gradient approach to inverse scattering for binary objects in stratified media,” *Inverse Probl.*, vol. 12, no. 4, pp. 463–481, 1996, doi: 10.1088/0266-5611/12/4/009.

[23] T. Isernia, V. Pascazio, and R. Pierri, “A nonlinear estimation method in tomographie imaging,” *IEEE Trans. Geosci. Remote Sens.*, vol. 35, no. 4, pp. 910–923, 1997, doi: 10.1109/36.602533.

[24] P. M. van den Berg and R. E. Kleiman, “A contrast source inversion method,” *Inverse Probl. 13 1607*, vol. Inv. Probl, 1997.

[25] L. Di Donato, M. T. Bevacqua, L. Crocco, and T. Isernia, “Inverse Scattering Via Virtual Experiments and Contrast Source Regularization,” *IEEE Trans. Antennas Propag.*, vol. 63, no. 4, pp. 1669–1677, 2015, doi: 10.1109/TAP.2015.2392124.

[26] I. Catapano, L. Crocco, M. D’Urso, and T. Isernia, “On the effect of support estimation and of a new model in 2-D inverse scattering problems,” *IEEE Trans. Antennas Propag.*, vol. 55, no. 6 II, pp. 1895–1899, 2007, doi: 10.1109/TAP.2007.898647.

[27] M. Brignone, G. Bozza, A. Randazzo, M. Piana, and M. Pastorino, “A hybrid approach to 3D microwave imaging by using linear sampling and ACO,” *IEEE Trans. Antennas Propag.*, vol. 56, no. 10, pp. 3224–3232, 2008, doi: 10.1109/TAP.2008.929504.

[28] I. Catapano, L. Crocco, M. D. Urso, and T. Isernia, “3D microwave imaging via preliminary support reconstruction: Testing on the Fresnel 2008 database,” *Inverse Probl.*, vol. 25, no. 2, 2009, doi: 10.1088/0266-5611/25/2/024002.

[29] F. Cakoni, D. Colton, and P. Monk, “Qualitative methods in inverse electromagnetic scattering theory: Inverse scattering for anisotropic media,” *IEEE Antennas Propag. Mag.*, vol. 59, no. 5, pp. 24–33, 2017, doi: 10.1109/MAP.2017.2731662.

[30] F. Cakoni, D. Colton, and P. Monk, “The linear sampling method in inverse electromagnetic scattering,” *CBMS-NSF Reg. Conf. Ser. Appl. Math.*, no. 80, pp. 1–136, 2011, doi: 10.1137/1.9780898719406.

[31] A. Kirsch, “Characterization of the shape of a scattering obstacle using the spectral data of the far field operator,” *Inverse Probl.*, vol. 14, no. 6, pp. 1489–1512, 1998, doi: 10.1088/0266-5611/14/6/009.

[32] Constantine A. Balanis, *ADVANCED ENGINEERING ELECTROMAGNETICS*, 2nd ed. John Wiley & Sons, Inc., 2012.

[33] I. Catapano, L. Crocco, and T. Isernia, “On simple methods for shape reconstruction of unknown scatterers,” *IEEE Trans. Antennas Propag.*, vol. 55, no. 5, pp. 1431–1436, 2007, doi: 10.1109/TAP.2007.895563.

[34] D. Colton and R. Kress, “Inverse acoustic and electromagnetic scattering theory: Fourth edition,” *Appl. Math. Sci.*, vol. 93, pp. 1–514, 1992.

[35] M. Bertero and P. Boccacci, “INTRODUCTION TO INVERSE PROBLEMS IN IMAGING Institute of Physics Publishing Bristol and Philadelphia Contents,” *Bristol, U.K. Inst. Phys.*, pp. 15–58, 1998.

[36] G. H. Golub and C. F. Van Loan, *Matrix Computations*. 1998.

[37] L. Crocco, L. Di Donato, I. Catapano, and T. Isernia, “An improved simple method for imaging the shape of complex targets,” *IEEE Trans. Antennas Propag.*, vol. 61, no. 2, pp. 843–851, 2013, doi: 10.1109/TAP.2012.2220329.

[38] I. Catapano and L. Crocco, “An imaging method for concealed targets,” *IEEE Trans. Geosci. Remote Sens.*, vol. 47, no. 5, pp. 1301–1309, 2009, doi: 10.1109/TGRS.2008.2010773.

[39] K. Agarwal, X. Chen, and Y. Zhong, “A multipole-expansion based linear sampling method for solving inverse scattering problems,” *Opt. Express*, vol. 18, no. 6, p. 6366, 2010, doi: 10.1364/oe.18.006366.

[40] X. Chen and Y. Zhong, “MUSIC electromagnetic imaging with enhanced resolution for small inclusions,” *Inverse Probl.*, vol. 25, no. 1, 2009, doi: 10.1088/0266-5611/25/1/015008.

[41] A. F. Oskooi, D. Roundy, M. Ibanescu, P. Bermel, J. D. Joannopoulos, and S. G. Johnson, “Meep: A flexible free-software package for electromagnetic simulations by the FDTD method,” *Comput. Phys. Commun.*, vol. 181, no. 3, pp. 687–702, 2010, doi: 10.1016/j.cpc.2009.11.008.